JACS
JOURNAL OF THE AMERICAN CHEMICAL SOCIETY
pubs.acs.org/JACS
Article

# A Change of Pace: Record Photoresponse through Spirooxazine Confinement in a Metal−Organic Matrix

Grace C. Thaggard, Gina R. Wilson, Mamata Naik, Molly A. Quetel, Jaewoong Lim, Buddhima K. P. Maldeni Kankanamalage, Mark D. Smith, and Natalia B. Shustova*

Cite This: J. Am. Chem. Soc. 2024, 146, 31746−31756
Read Online



**ABSTRACT:** Modern and upcoming high-speed optoelectronics as well as secure data storage or solar energy harvesting technologies integrating stimuli-responsive materials fully rely on the fundamental concept of rapid transitions between discrete states possessing different properties. Relatively slow transition kinetics between those states for commonly used classes of photochromic compounds in solution or bulk solids severely restrict the applicability of stimuli-responsive materials for device development. Herein, we report a multivariate strategy based on a photochromic spirooxazine derivative, coordinatively integrated in the solvent-free confined space of a solid-state matrix, such as a metal−organic framework (MOF), for the first time, resulting in the fastest photoresponse reported for any solid-state material to date. The photoisomerization rate for the developed photochromic material was estimated to be 126 $s^{-1}$, surpassing any literature reports to the best of our knowledge. We also shed light on the fundamentals of the correlation between framework topology, the nature of organic linkers, and the presence/absence of organic solvent within the scaffold voids on the material photoresponse using a series of isoreticular frameworks. Overall, the presented conceptual approach allows for tailoring the isomerization kinetics of photochromic molecules in the solid state over a range of 4 orders of magnitude—an unprecedented span that provides a pathway for addressing challenges associated with the response rate and photoisomerization, which are key criteria in stimuli-responsive material development.

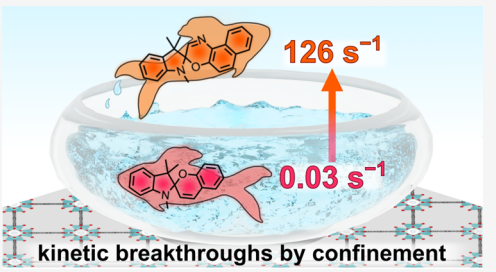




## INTRODUCTION

Modern high-speed optoelectronics,[1−6] data encryption and storage technologies,[7−13] as well as solar energy-related applications utilizing stimuli-responsive materials, require rapid and reversible kinetics, i.e., fast switching between two or more discrete states.[14−19] Such rapid switching allows for efficient control of the material properties including, for instance, modulating conductivity or tailoring optical profile.[20−24] However, many of the commonly used photochromic molecules (e.g., hydrazone or spiropyran derivatives[25−27]) exhibit limited isomerization in the solid state mainly due to strong intermolecular interactions imposed by molecular close packing in bulk solids, which severely restricts their applicability in device development.[6,27,28] Therefore, integration of photochromic molecules into modular and synthetically programmable porous matrices, such as metal−organic frameworks (MOFs)[29−53] could be used as a powerful concept for promoting rapid isomerization kinetics of sterically demanding photoswitches in the solid state.[27,54−60]

Despite advances in photochromic material performance due to photoresponsive moiety integration within MOFs, the aforementioned applications, and especially, the future technological breakthroughs will likely be based on isomerization kinetics that surpass the rate values reported for "unconstrained" conventional photochromic molecules even in solution.[5,28,61] Thus, there is an urgent need for groundbreaking discoveries, capable of pushing the current benchmark isomerization rates to the next level.

Among the possible conceptual solutions for addressing this challenge are (i) designing novel classes of photochromic building blocks that intrinsically exhibit rapid switching or (ii) engineering the second sphere interactions around stimuli-responsive moieties to support rapid photoisomerization kinetics (Scheme 1). In these studies, we realized both concepts (i and ii), resulting in a difference in photoisomerization rates of more than 3 orders of magnitude, allowing us to surpass the photochromic performance of any photochromic molecule in the solid state or solution reported to date (Scheme 1 and Figure 1).

In particular, the integration of a spirooxazine-based derivative (1,3,3-trimethylspiro[indoline-2,3′-naphtho[2,1-*b*]-[1,4]oxazine]-5-carboxylic acid (CSO)), which is commonly known for rapid solution-based kinetics and fatigue resist-

Received: August 3, 2024
Revised: October 27, 2024
Accepted: October 28, 2024
Published: November 6, 2024





https://doi.org/10.1021/jacs.4c10636
J. Am. Chem. Soc. 2024, 146, 31746−31756

**Scheme 1. Schematic Representation of More Than 3 Orders of Magnitude Difference between Photoisomerization Rates Achieved for a Commonly Used Spiropyran Derivative (SP) in Solution in *N,N*-Dimethylformamide (DMF) and a Spirooxazine-Based Compound (SPO) Confined through Coordination within the Pores of an Evacuated Framework; Resulting in the Record Value Reported for Any Photochromic Compound in the Solid State or Solution to Date**

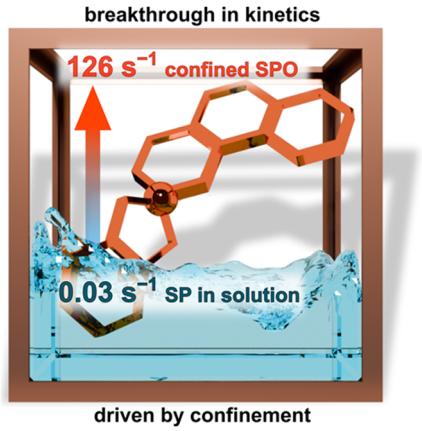


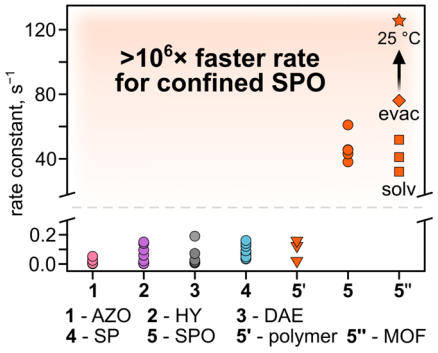


**Figure 1.** Plot demonstrating the photoisomerization rate constants for common classes of photochromic compounds (data from this work presented by orange circles, squares, diamond, and star): azobenzene (AZO, pink), hydrazone (HY, purple), diarylethene (DAE, gray), and spiropyran (SP, blue) in solution,[10,23,57,58,61−69] as well as spirooxazine derivatives in solution (orange circles), integrated within polymers (orange triangles),[70] and in MOFs. Data collected for the MOFs containing solvent molecules in the pores are represented by orange squares (UiO-67 + CSO, UiO-68 + CSO, and NU-1000 + CSO at 8 °C), for the solvent-free MOF (UiO-67 + SPO at 8 °C) represented by the orange diamond, and for solvent-free MOF (estimated at 25 °C) represented by the orange star. Tables 1 and S2 contain the rate constants corresponding to the presented data. The >$10^6$-fold rate enhancement for confined SPO at 25 °C ($k$ = 126 $s^{-1}$) relates to comparison with azobenzene in an ethanol solution ($k$ = 3.2 × $10^{-5}$ $s^{-1}$).[64]

ance,[71−73] within an engineered MOF environment resulted in the achievement of a 126 $s^{-1}$ isomerization rate constant. This value surpasses isomerization rate constants reported for any commonly used photochromic molecules, for instance, azobenzene derivatives, in solution such as dimethyl sulfoxide by 2520-fold (e.g., $k_{azobenzene,DMSO}$ = 0.05 $s^{-1}$ versus $k_{(UiO\text{-}67+CSO)}$ = 126 $s^{-1}$ for solvent-free UiO-67 + CSO at 25 °C).[62] The prepared photochromic material is also the first example of the stimuli-responsive material with spirooxazine coordinatively integrated within a well-defined porous scaffold.

We also placed the observed advanced photochromic performance of the spirooxazine compound in context with commonly reported analogs like spiropyran derivatives based on the in-depth photophysical analysis performed for spirooxazine-based materials for the first time. On the examples of two photochromic compounds belonging to two distinct classes, we demonstrated the concept of scaffold-imposed photoisomerization kinetics of photochromic moieties within the confined environment of three isoreticular MOFs (12−23 Å pore sizes) as well as a framework possessing a completely different structural topology. Comprehensive photophysical studies using time-resolved and steady-state ultraviolet−visible (UV−vis) and diffuse reflectance spectroscopies, supported by thorough material characterization by single-crystal and powder X-ray diffraction (PXRD), as well as nuclear magnetic resonance (NMR) spectroscopic studies, demonstrate a multivariate approach to photochromic material design and provide a viable pathway to significant breakthroughs in the area of photochromic materials, possessing the most rapid photoresponse reported to date (e.g., 4200-fold rate enhancement: commonly applied spiropyran derivatives with $k_{CSP,DMF}$ = 0.03 $s^{-1}$ in comparison with $k_{UiO\text{-}67+CSO(evac)}$ = 126 $s^{-1}$ for solvent-free UiO-67 + CSO at 25 °C[6,27,61,74−76]).

## RESULTS AND DISCUSSION

As the central photochromic moiety for our studies, we selected spirooxazine derivatives due to their excellent fatigue resistance and more rapid switching kinetics in comparison with their close well-studied photochromic analogs such as spiropyran-based compounds (Figure 1).[27,76−79] In the case of spirooxazine-based compounds, the fast switching kinetics is attributed to the presence of the additional nitrogen atom in their structure (Figure 2). Such structural changes result in a lower energy barrier for rotation around a C═N bond compared to the energy required for rotation around a C═C bond in spiropyran derivatives.[79] Despite these facts, there are very few studies that have evaluated the photophysical properties of spirooxazine derivatives, especially within well-defined solid-state host matrices, in comparison with other classes of photochromic molecules such as azobenzene.[54−56,80−83] For instance, there are over 3550 reports of azobenzene-based materials, while less than 130 describe spirooxazine compounds to date, the majority of which focus on polymers or self-assembled monolayers.[72,84−88] Thus, besides breakthroughs in photochromic material performance, these studies also fill the gaps in the fundamental understanding of the photophysical behavior of spirooxazine derivatives in general.

As a first step, we synthesized a carboxylic acid-functionalized spirooxazine derivative, 1,3,3-trimethylspiro[indoline-2,3′-naphtho[2,1-*b*][1,4]oxazine]-5-carboxylic acid (CSO, Figures 2 and 3).[71,89] The detailed synthetic procedures for CSO preparation and purification, as well as full characterization by $^1$H and $^{13}$C NMR spectroscopies, high-resolution mass spectrometry, and single-crystal X-ray diffraction, are given in the Supporting Information (SI, Figures S1−S3). In addition, a previously reported spiropyran derivative, 1′,3′,3′-trimethyl-6-nitrospiro[chromene-2,2′-indoline]-5′-carboxylic acid (CSP, Figure 2) was prepared based on a literature procedure.[61] Both CSO and CSP structures possess the reactive functional groups (e.g., −COOH) to facilitate the preparation of stimuli-


https://doi.org/10.1021/jacs.4c10636
J. Am. Chem. Soc. 2024, 146, 31746−31756

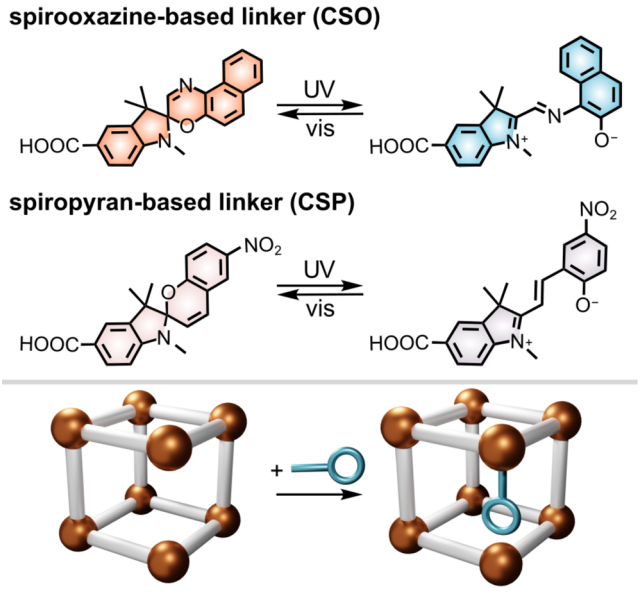


**Figure 2.** (top) Carboxylic acid-functionalized spirooxazine (CSO, orange) and spiropyran (CSP, light pink) derivatives used for material preparation. Both compounds undergo photoisomerization forming merocyanine isomers of CSO (blue) and CSP (light purple). (bottom) Schematic representation of photoswitch (blue) integration through coordination to a MOF's unsaturated metal nodes (copper spheres).

responsive materials through postsynthetic installation at the coordinatively unsaturated metal nodes of several Zr-based MOFs as discussed below (Figure 2).[57,61,90]

The spiropyran derivative, CSP, was discussed within the frame of the presented studies to place the photoresponsive behavior of spirooxazine-containing materials in context with the scientific literature by comparison with a more extensively studied class of photochromic compounds with a similar photoisomerization mechanism.[27,91] Both classes of compounds undergo photoisomerization from a neutral isomer to a charge-separated merocyanine isomer through an excited state C−O bond cleavage (Figure 2).[27,91] Therefore, we hypothesize that similar to spiropyran derivatives,[92−96] prepared CSO confined within the framework matrix provides the opportunity for tailoring of photochromic kinetics through solvent molecules filling the MOF pores since switching rates are prone to be sensitive to the solvent polarity and viscosity.[92,93,97,98] Especially in the case of spiropyran derivatives as previously reported,[61,92−95] the solvent-dependent nature of the photoisomerization rates has to be taken into account because of the formation of strong electrostatic interactions between the merocyanine isomers and polar solvents, which could significantly affect merocyanine-to-spirooxazine isomerization kinetics.[99,100]

For the integration of the selected photochromic moieties, we have selected scaffolds (i.e., MOFs) based on the following criteria. First, the framework should possess open coordination sites for postsynthetic anchoring of CSO or CSP. Second, the selected scaffold should possess intrinsic voids that can accommodate structural rearrangements associated with the photoisomerization of sterically demanding photochromic molecules. Finally, the chosen matrix should maintain structural integrity after its postsynthetic modification[101] with a photochromic unit and its exposure to UV and visible light during the subsequent photophysical experiments. As a result, four Zr-based MOFs were probed for photochromic unit integration as shown in Figure 3 due to their broad thermal and chemical stability, the presence of open coordination sites to promote photoswitch integration, and sufficient pore sizes to accommodate the structural rearrangement associated with photoisomerization of the selected spirooxazine and spiropyran derivatives. In particular, $Zr_6O_4(OH)_4(TA)_6$ (TA = terephthalic acid, UiO-66; UiO = University of Oslo), $Zr_6O_4(OH)_4(BPDC)_6$ ($H_2BPDC$ = 1,4-biphenyldicarboxylic acid, UiO-67), and $Zr_6O_4(OH)_4(NBB)_6$ ($H_2NBB$ = 4,4′-(naphthalene-1,4-diyl)dibenzoic acid, UiO-68) belong to an isostructural series of MOFs known to possess defect sites (i.e., absence of an organic linker) which could allow for integration of CSO and CSP (Figure 2). As illustrated in Figure 3, UiO-66, −67, and −68 have identical pore geometries, but their dimensions increase in the order of UiO-66 < UiO-67 < UiO-68. Based on the geometric considerations of the scaffolds and CSO, UiO-66 was selected as a control (vide infra). Thus, the choice of the UiO-series MOFs as platforms for photoswitch integration allowed us to probe potential confinement effects on CSO photoisomerization without the complicating influence of different organic linkers that could interact with the photochromic unit or significant differences in pore topology. As the fourth framework, we synthesized $Zr_6O_4(OH)_8(TBAPy)_2$ ($H_4TBAPy$ = 1,3,6,8-tetrakis(*p*-benzoic acid)pyrene, NU-1000; NU = Northwestern University),

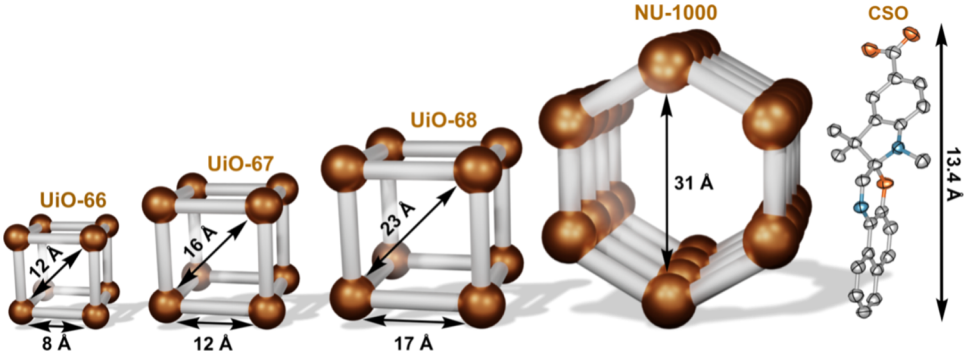


**Figure 3.** Schematic representation of the four frameworks used to probe the effect of confinement on CSP and CSO photoisomerization kinetics, as well as the X-ray crystal structure of CSO. Displacement ellipsoids are presented at the 80% probability level, and hydrogen atoms are omitted for clarity. The estimated pore dimensions of each MOF and the length of CSO are highlighted. X-ray crystal structures of each MOF are given in Figures S57−S60.



https://doi.org/10.1021/jacs.4c10636
J. Am. Chem. Soc. 2024, 146, 31746−31756

possessing much larger the pore size in comparison with the UiO series (Figure 3 and S57−S60).

All of the mentioned parent frameworks (i.e., UiO-66, UiO-67, UiO-68, and NU-1000) were synthesized via solvothermal methods as reported in the literature.[102−104]

Prior to photoswitch integration, MOF crystallinity and integrity were evaluated through PXRD analysis (Figures S10−S15). The average number of defects per metal node for UiO-67 and UiO-68 was estimated based on a reported literature procedure using thermogravimetric analysis (TGA, Figures S49 and S50).[90,105] Following framework characterization, CSO and CSP were postsynthetically integrated within each MOF by heating the MOF powders in 60 mM solutions of either CSO or CSP in *N*,*N*-dimethylformamide (DMF) at 80 °C for 3 days (see more details in the SI).

After photoswitch installation, the photochromic MOFs were thoroughly washed with DMF over 3 days to remove any uncoordinated CSO or CSP from the framework pores or bound to the surface. The resulting spirooxazine- and spiropyran-containing materials were reanalyzed using PXRD to confirm structural integrity (Figures S10−S15). The amount of photoswitch installed in each sample was estimated based on $^1$H NMR spectroscopic analysis of the digested MOF samples (destroyed in the presence of acid; see SI for more details; Figures S4−S9).

Following material synthesis and characterization, we began the photophysical studies of spirooxazine-based frameworks by evaluating the photoisomerization of CSO in the solution used in the presented work as a reference (Figure 4 and Table 1).

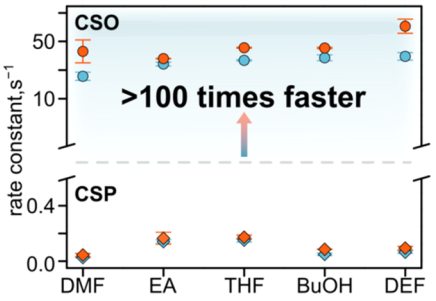


**Figure 4.** Plot demonstrating the photoisomerization rate constants for CSO (circles) and CSP (diamonds) in solution. Rate constants determined at 25 °C are depicted in orange, while those determined at 8 °C are depicted in blue. The error bars represent the standard deviation calculated for at least three trials.

For this, a series of organic solvents of varying polarity were selected since it is known in the literature that solvent-photoswitch interactions (e.g., dipole−dipole or hydrogen bonding interactions) can significantly impact photoisomerization kinetics.[94,95] Specifically, we anticipated that more polar solvents (e.g., DMF) would stabilize the zwitterionic merocyanine isomers and could slow the merocyanine-to-spirooxazine photoisomerization kinetics.[99,100]

Photoisomerization kinetics of CSO and CSP in DMF, tetrahydrofuran (THF), *N*,*N*-diethylformamide (DEF), butanol (BuOH), and ethyl acetate (EA) was evaluated using time-resolved UV−vis spectroscopy (Table 1). For this, each solution was exposed to a 365-nm excitation wavelength for 30 s to promote the formation of the colored merocyanine isomer which exhibits a characteristic strong absorbance band centered around 590 nm. The exact value of $\lambda_{max}$ is solvent-dependent (Figure S62 and Table S2), and the UV−vis absorbance spectra for CSO in solution exhibit a bathochromic shift as a function of increasing solvent polarity, which is in line with previous literature reports suggesting that interactions with polar solvent molecules stabilize merocyanine isomers.[100]

**Table 1. Summary of Photoisomerization Kinetics Data**

| sample | conditions | *T*, °C | *k*, s$^{-1}$ |
|---|---|---|---|
| CSO[a] | DMF | 8 | 26 ± 3 |
| CSO[a] | DMF | 25 | 43 ± 8 |
| CSO[a] | THF | 8 | 37 ± 1 |
| CSO[a] | THF | 25 | 46 ± 1 |
| CSO[a] | DEF | 8 | 40 ± 3 |
| CSO[a] | DEF | 25 | 61 ± 5 |
| CSO[b] | BuOH | 8 | 39 ± 2 |
| CSO[b] | BuOH | 25 | 45 ± 1 |
| CSO[a] | EA | 8 | 34 ± 1 |
| CSO[a] | EA | 25 | 38 ± 1 |
| UiO-68 + CSO | DMF | 8 | 41 ± 4 |
| UiO-68 + CSO | DMF | 25 | 62 + 5 |
| NU-1000 + CSO | DMF | 8 | 53 ± 5 |
| UiO-67 + CSO | DMF | 8 | 32 ± 4 |
| UiO-67 + CSO | 2 h evac. | 8 | 38 ± 2 |
| UiO-67 + CSO | 4 h evac. | 8 | 42 ± 2 |
| UiO-67 + CSO | 6 h evac. | 8 | 53 + 2 |
| UiO-67 + CSO | 24 h evac. | 8 | 76 + 4 |
| CSP[a] | DMF | 8 | (2.6 ± 0.3) × 10$^{-2}$ |
| CSP[a] | DMF | 25 | (4.0 ± 1.0) × 10$^{-2}$ |
| CSP[a] | THF | 8 | (1.5 ± 0.1) × 10$^{-1}$ |
| CSP[a] | THF | 25 | (1.7 ± 0.1) × 10$^{-1}$ |
| CSP[a] | DEF | 8 | (6.4 ± 0.9) × 10$^{-2}$ |
| CSP[a] | DEF | 25 | (9.0 ± 1.0) × 10$^{-2}$ |
| CSP[b] | BuOH | 8 | (4.9 ± 0.9) × 10$^{-2}$ |
| CSP[b] | BuOH | 25 | (8.6 ± 0.1) × 10$^{-2}$ |
| CSP[a] | EA | 8 | (1.4 ± 0.2) × 10$^{-1}$ |
| CSP[a] | EA | 25 | (1.6 ± 0.4) × 10$^{-1}$ |
| UiO-67 + CSP | DMF | 8 | (4.6 + 0.4) × 10$^{-2}$ |
| UiO-67 + CSP | DMF | 25 | (6.1 ± 0.4) × 10$^{-2}$ |
| UiO-68 + CSP | DMF | 25 | (7.3 ± 0.4) × 10$^{-2}$ |
| NU-1000 + CSP | DMF | 25 | (1.1 ± 0.1) × 10$^{-1}$ |

[a]Measurements performed using 3.0 mM solutions. [b]Measurements performed using 1.9 mM solutions.

Next, the samples were exposed to $\lambda_{ex}$ = 400−900 nm, and the attenuation of the band centered at 590 nm was monitored as a function of time, corresponding to merocyanine-to-spirooxazine (or merocyanine-to-spiropyran in the case of CSP) photoisomerization (Figures 2 and S16−S35). Fitting the acquired absorbance data with a first-order exponential decay equation based on previous literature reports[58,105] allowed for the estimation of the photoisomerization rate constants, *k* (see the SI for a more detailed explanation of the data fitting and kinetic model analysis). Since the reported photoisomerization rates for spirooxazine derivatives are much faster than other classes of photochromic compounds like spiropyran (Figure 1), the measurements were performed below 25 °C to reduce the photoisomerization rate and to allow for a more accurate data analysis. In addition, CSO installed in the confined space of MOFs (vide infra) exhibited isomerization rates that are close to the limit of handling them using the current setup (including manual switching for the collection of the first data point), and therefore, for each solution, the described experiments were performed in both a



https://doi.org/10.1021/jacs.4c10636
J. Am. Chem. Soc. 2024, 146, 31746−31756

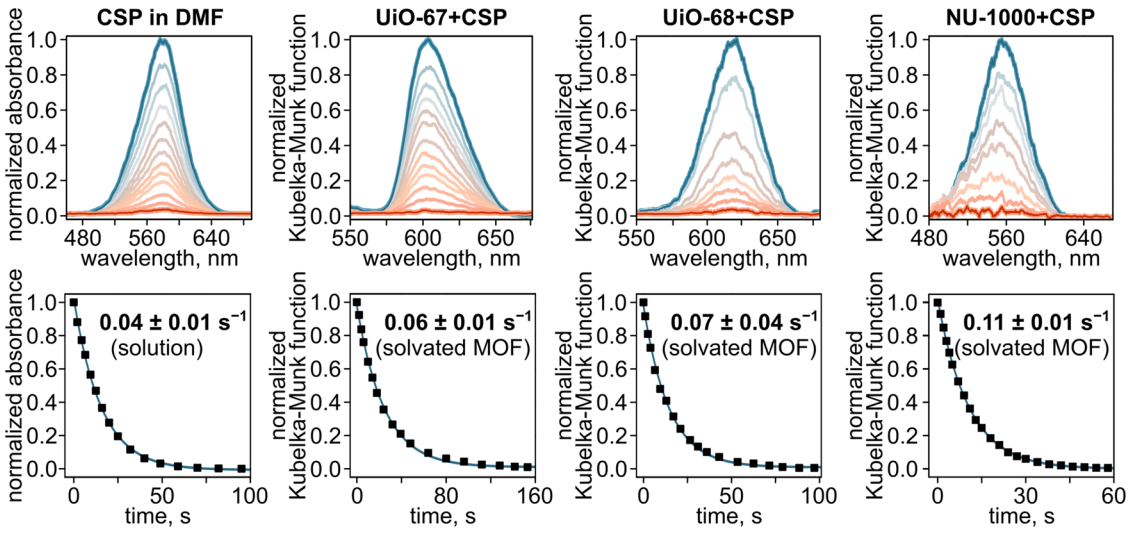


**Figure 5.** (top) UV−vis absorbance spectra of CSP in solution, as well as diffuse reflectance spectra of the UiO-67 + CSP, UiO-68 + CSP, and NU-1000 + CSP frameworks. The gradient from blue to orange represents photoisomerization from merocyanine to spiropyran forms. (bottom) Kinetic plots of CSP in solution and integrated within each MOF matrix, demonstrating the influence of host framework on photoisomerization kinetics.

cold room carefully maintained at 8 and at 25 °C for reliable comparison with the acquired MOF data and previously reported literature values.[23,58,61,70] The determined temperature-dependent rate constants could then be used to approximate the activation energy for the photoisomerization process (described below as well in the SI in more detail). The UV−vis absorbance spectra and kinetic plots for every measured sample can be found in the SI (Figures S16−S35).

As shown in Figure 4 and corresponding Table 1, the estimated rate constants for CSO in solution at 25 °C ranged from 43 to 61 $s^{-1}$, demonstrating that prepared CSO possesses a photoresponse which is between 100−1000 times faster in comparison with that of CSP ($k_{CSP}$ = 0.026−0.17 $s^{-1}$). Thus, the initial solution-based studies showcase the nearly untapped potential of spirooxazine derivatives, providing a strong foundation to explore their behavior within a MOF matrix, allowing for the elimination of CSO-intermolecular interactions as shown below. Photophysical experiments involving the photochromic MOF samples were conducted similarly as described for the solution studies above by time-resolved diffuse reflectance spectroscopy. However, one notable difference was that the photoisomerization kinetics data for CSO-containing MOFs could only reasonably be collected at 8 °C because of difficulties in detecting the rapid attenuation occurring at 25 °C (Table 1, S2 and S3).

As a starting point, we investigated the possibility of integrating CSO within the UiO-66 matrix which possesses the smallest pore size among the UiO series MOFs. As shown in Figure 3, the CSO structure possesses 6.4 × 13.4 Å dimensions, while UiO-66 possesses 8 × 12 Å pores. Therefore, there is only one way for the CSO molecule to fit the pores of the UiO-66 matrix: through the 8-Å channels. However, our attempts to integrate CSO within the UiO-66 matrix using different synthetic protocols were unsuccessful according to $^1$H NMR spectroscopic analysis of the digested MOF sample and diffuse reflectance spectroscopic studies. Thus, we used UiO-66 as a control for the subsequent photophysical analysis of other samples described below.

As a next step, we used UiO-67 possessing larger pore sizes of 12 × 16 Å which are more compatible with the size of CSO (Figure 3). As a result, we confirmed the integration of CSO by $^1$H NMR spectroscopic analysis of the digested samples (Figure S4) as well as diffuse reflectance spectroscopic studies (Figures 6 and S42). Furthermore, changes in the sample color, from beige to dark blue, upon spirooxazine integration within the MOF and further exposure to UV light could be easily detected visually by the naked eye (Figure S61). For comparison and as a control experiment, we similarly integrated the CSP derivative within the UiO-67 scaffold.

Next, the photoisomerization kinetics of UiO-67 + CSO and UiO-67 + CSP as-synthesized (i.e., containing DMF molecules in the MOF pores) were measured by time-resolved diffuse reflectance spectroscopy. The resulting rate constants, $k_{UiO\text{-}67,DMF}$ and $k_{UiO\text{-}67,DMF}$, measured at 8 °C were found to be 32 ± 4 and 0.046 ± 0.004 $s^{-1}$ for CSO and CSP, respectively (Figures 5 and 6). As expected, the rate constants determined for as-synthesized UiO-67 + CSO and UiO-67 + CSP (i.e., MOFs containing DMF molecules in their pores) are in line with the rate constants determined for the same photochromic compounds in a DMF solution (Table 1). For instance, the found rate constants for CSO in a DMF solution is 26 ± 3 $s^{-1}$ while the one for UiO-67 + CSO containing DMF molecules within its pores is 32 ± 4 $s^{-1}$. Likewise, the rate constant values for CSP (3 mM in DMF) and UiO-67+CSP in the presence of DMF were 0.026 ± 0.003 and 0.046 ± 0.004 $s^{-1}$, respectively. Moreover, similar to UV−vis studies performed for CSO in solution (vide supra), a bathochromic shift in the diffuse reflectance profile of UiO-67 + CSO was observed upon its submersion in solvents of increasing polarity (such as ethyl acetate, DMF, or ethanol, Figure S63); demonstrating the similar trend that the solvent-photoswitch interactions occurring within the MOF pores allow for stabilization of the merocyanine isomer as described above. Optical cycling experiments performed on UiO-67 + CSO demonstrate the maintenance of the detected rate constant across at least six cycles (Figure S48). Notably, the sample structural integrity was confirmed by PXRD analysis after photophysical measurements (Figures S10−S15) including optical cycling.


https://doi.org/10.1021/jacs.4c10636
J. Am. Chem. Soc. 2024, 146, 31746−31756

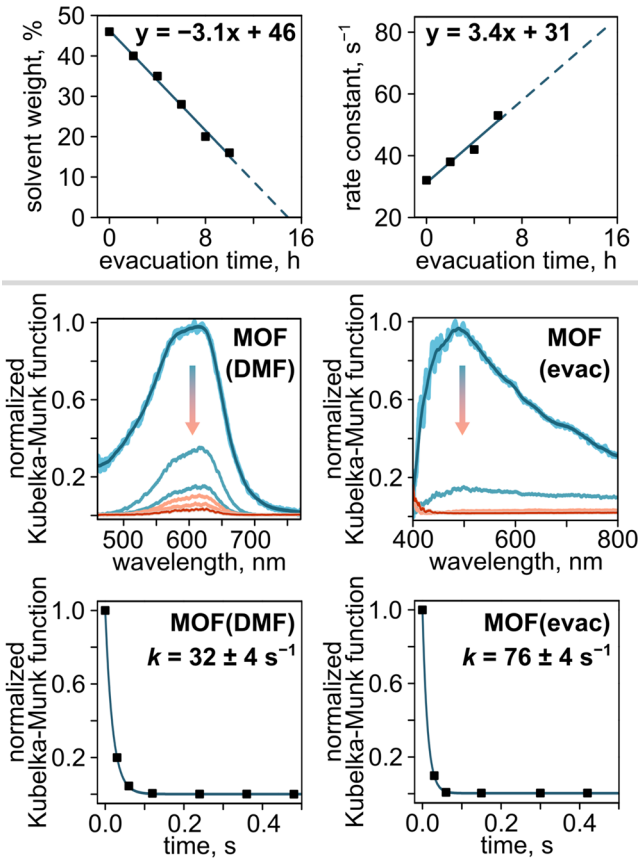


**Figure 6.** (top) Plots demonstrating the change in solvent weight loss based on TGA (left) and photoisomerization rate constant for UiO-67 + CSO (right) as a function of evacuation time. (middle, bottom) Diffuse reflectance spectra and photoisomerization kinetics plots for UiO-67 + CSO as-synthesized (left) and after evacuation for 24 h (right).

We continued our investigation by probing the photophysical behavior of CSO and CSP integrated within two scaffolds with pore sizes exceeding UiO-67 ones, such as UiO-68 and NU-1000 (Figure 3) hypothesizing that an increase in the pore size could potentially reduce the steric hindrance around the photochromic moiety. Besides that, a few literature reports have already shown that the photophysical response of photochromic molecules can be impacted by the cavity size of a host matrix (e.g., metal−organic cages[60,96,106,107] or MOFs[108,109]), which provides a foundation for the hypothesis that the switching rate of integrated photochromic units could be enhanced through increased pore size. Therefore, we tested the photophysical behavior of a photochromic moiety integrated within frameworks of different sizes. As a result, the comparative analysis of the photoisomerization rate constants for as-synthesized UiO-67 + CSO and UiO-68 + CSO at 8 °C revealed an increased rate as a function of pore size. For instance, the rate constant for CSO integrated in UiO-68 was determined to be 41 ± 4 $s^{-1}$, which is approximately 1.3-fold faster than UiO-67 + CSO (and ∼850-fold faster than UiO-68 + CSP estimated at 8 °C). Likewise, the photoisomerization rate constant for UiO-68 + CSP was 1.2-fold higher than that of UiO-67 + CSP measured at 25 °C (Table 1 and Figure 5).

To probe possible confinement effects further, the photoisomerization rate constants of NU-1000 + CSO and NU-1000 + CSP were also measured since NU-1000 possesses an even larger pore diameter (∼31 Å) than UiO-68 (∼23 Å). As expected based on the acquired results for photochromic units integrated in UiO-68, we detected an increase in the rate constant for both CSO and CSP integrated in NU-1000 compared to the other frameworks used herein (Figures 5 and S47). For instance, the estimated rate constant for NU-1000 + CSO at 8 °C was 53 ± 5 $s^{-1}$, which is 1.7- and 1.3-fold higher than the rate constants determined for CSO integrated in UiO-67 and UiO-68 at the same temperature, respectively. The same trend was observed in the case of NU-1000 + CSP, which possesses a photoisomerization rate constant that is 1.8- and 1.5-fold higher than UiO-67 + CSP and UiO-68+CSP, respectively (Table 1 and Figure 5). Notably, the previous reports of a similar spiropyran derivative integrated into covalent-organic frameworks (COFs) possessing a similar pore size to that of NU-1000 (e.g., ∼31 Å versus ∼33 Å) demonstrated restricted photoisomerization of the spiropyran unit due to strong noncovalent interactions between the photoswitch and the COF pore wall.[57] In the same vein, studies by Klajn and co-workers demonstrated that the photoresponse of spiropyran derivatives integrated within metal−organic cages is dependent on not only the size of the cage cavity but also the pore geometry and organic linker functionalities.[96] Thus, the presented studies in combination with the previous literature reports, clearly demonstrate that photoisomerization kinetics is dependent on variable parameters and/or their combination (e.g., pore size or presence/absence of solvent in this work). For instance, it depends not only on the class of photochromic compound (e.g., spirooxazine versus spiropyran) and matrix pore size but also on the possible photoswitch-framework intermolecular interactions.[60,61,96,110] As such, targeting a particular range of photoisomerization rates can only be achieved through a multivariate approach considering all of the mentioned factors as a whole.[24,57,61,96,108−111]

As a final strategy for modulating the photoisomerization rate of CSO-based materials, we evaluated whether the absence of solvent-switch intermolecular interactions could destabilize the merocyanine isomer and enhance the merocyanine-to-spirooxazine photoisomerization rate (Scheme 1 and Figure 6). To test this hypothesis, UiO-67 + CSO was evacuated for 2−24 h prior to its analysis by diffuse reflectance spectroscopy at 8 °C. The choice of this MOF for evaluation of the rates of a confined photochromic moiety without the presence of the solvent molecules was mainly due to framework stability upon its evacuation. Special precautions were taken to ensure that the MOF powders were not exposed to air before or during each measurement (more specific information about measurement details is provided in the SI).

Initially, we found the degree-of-pore-solvation-isomerization-rate correlation, which also allows us to approximate the time necessary for the complete evacuation of synthesized UiO-67 + CSO. As shown in Figures 6 and S51−S56, TGA was used to estimate the weight loss due to solvent evaporation upon heating for each UiO-67 + CSO sample with a known evacuation time. As expected, we detected an increase in the photoisomerization rate constants for UiO-67 + CSO as a function of evacuation time (Table 1 and Figure 6). For instance, the rate constant increased almost twice from $k_{\text{UiO-67,evac}}$ = 38 ± 2 $s^{-1}$ after 2h-evacuation to $k_{\text{UiO-67,evac}}$ = 76 ± 4 $s^{-1}$ after evacuation for 24 h (Figures 6 and S42−S46). In comparison, literature reports of a spiropyran derivative


https://doi.org/10.1021/jacs.4c10636
J. Am. Chem. Soc. 2024, 146, 31746−31756

integrated in solvent-free confined space estimated the photoisomerization rate constant to be ~31 $s^{-1}$.[61] Notably, the evacuated MOF samples maintained structural integrity according to PXRD analysis (Figures S10−S15). To the best of our knowledge, these data represent the fastest reported photoisomerization rate constant for a solid-state material to date even considering experiments performed at room temperature.[61,85] Extrapolating the data shown in Figure 6 to a solvent content of 0% allowed us to estimate the time necessary for MOF complete evacuation which corresponds to approximately 16 h under vacuum. Thus, we estimate that UiO-67+CSO after 24 h of evacuation (Figure 6 and Table 1 and S3) can be considered as a close approximation of a solvent-free photoswitch environment.[61]

Encouraged by the forgoing results, we sought to estimate the rate constant for solvent-free UiO-67 + CSO at 25 °C as all measurements have been performed at 8 °C due to the rapid photoresponse (vide supra). For this, the activation energy ($E_a$) for the merocyanine-to-spirooxazine photoisomerization process was calculated for each solvent system according to the Arrhenius equation (see more details in the SI, eq S1). As a result, the average activation energy for DMF and DEF solvent systems (selected due to their similar dielectric constants) was found to be approximately 19 kJ/mol. Notably, the activation energy estimated based on the acquired photoisomerization kinetics data is in line with other literature reports of activation energies for spirooxazine derivatives.[112] With the rough assumption that the activation energy barrier is constant throughout the evacuation process, we evaluated that the rate constant for solvent-free UiO-67 + CSO at 25 °C is approximately 126 $s^{-1}$ as a conservative estimate (Figure 6). Therefore, the construction of a solvent-free environment around CSO, and likely other spirooxazine derivatives, is a pathway toward photoisomerization rates that cannot be attained in solution or upon integration in other solid-state matrices (e.g., polymers[84,91] or hydrogels[113]).

## CONCLUSIONS

The employed concept based on the CSO derivative, coordinatively integrated within a synthetically tunable environment of a solid matrix, resulted in the fastest photoresponse reported for any photochromic compound in the solid state or solution to date. The synthetically tailorable environment achieved through modularity of the confined environment in a MOF pore demonstrates a conceptual approach for surpassing the boundaries previously observed for solid-state photoisomerization of sterically demanding photochromic molecules. For the first time, we performed a detailed analysis of multiple variables affecting the photoisomerization kinetics of spirooxazine-containing materials on the example of a novel spirooxazine-based MOF, including the presence or absence of organic solvent, pore size, and framework topology. Moreover, investigating the influence of the choice of organic solvent on the switching kinetics of an underexplored class of photochromic compounds, spirooxazine derivatives, sheds light on the fundamentals of its intermolecular interactions with polar solvents, allowing for photoisomerization kinetics alternation. We successfully translated the fundamental knowledge acquired for a spirooxazine derivative in organic media to engineer a MOF environment in which the presence or absence of solvent molecules within pores could be used for tailoring the photoisomerization rate of integrated CSO units. As a result, we report one of the fastest photoisomerization rates for a solid-state material to date (over 2500 times faster than what is typically observed for photochromic molecules in solution (e.g., ~0.05 $s^{-1}$)[61,62]) which highlights a possible avenue for the use of photochromic materials in high-speed and ultraefficient optoelectronics devices. Combining the observed confinement effect with the construction of a solvent-free environment within MOF pores creates a generalizable strategy for targeting a particular photochromic performance (i.e., photoisomerization kinetics) for a desired application, which could range from high-resolution fluorescence microscopy based on photochromic tags[114−116] to photoisomerization rate-dependent anticounterfeiting technology,[12] high-speed optoelectronics, and beyond. We anticipate that such a powerful approach, allowing for tailoring the photoisomerization kinetics on demand through synthetically programmed frameworks, will usher in a new generation of functional materials that could have lasting impacts across the energy and technology sectors.

## ASSOCIATED CONTENT

### Supporting Information

The Supporting Information is available free of charge at https://pubs.acs.org/doi/10.1021/jacs.4c10636.

Additional experimental details, UV−vis; diffuse reflectance; and NMR spectra; TGA plots; and X-ray crystal structure refinement data; PXRD patterns (PDF)

### Accession Codes

Deposition Number 2374347 contains the supplementary crystallographic data for this paper. These data can be obtained free of charge via the joint Cambridge Crystallographic Data Centre (CCDC) and Fachinformationszentrum Karlsruhe Access Structures service.

## AUTHOR INFORMATION


### Corresponding Author

**Natalia B. Shustova** − *Department of Chemistry and Biochemistry, University of South Carolina, Columbia, South Carolina 29208, United States;* orcid.org/0000-0003-3952-1949; Email: shustova@sc.edu

### Authors

**Grace C. Thaggard** − *Department of Chemistry and Biochemistry, University of South Carolina, Columbia, South Carolina 29208, United States*

**Gina R. Wilson** − *Department of Chemistry and Biochemistry, University of South Carolina, Columbia, South Carolina 29208, United States*

**Mamata Naik** − *Department of Chemistry and Biochemistry, University of South Carolina, Columbia, South Carolina 29208, United States*

**Molly A. Quetel** − *Department of Chemistry and Biochemistry, University of South Carolina, Columbia, South Carolina 29208, United States*

**Jaewoong Lim** − *Department of Chemistry and Biochemistry, University of South Carolina, Columbia, South Carolina 29208, United States;* orcid.org/0000-0002-4557-0870

**Buddhima K. P. Maldeni Kankanamalage** − *Department of Chemistry and Biochemistry, University of South Carolina, Columbia, South Carolina 29208, United States*

**Mark D. Smith** − *Department of Chemistry and Biochemistry, University of South Carolina, Columbia, South Carolina 29208, United States*

Complete contact information is available at:
https://pubs.acs.org/10.1021/jacs.4c10636

### Author Contributions

The manuscript was written through contributions of all authors. All authors have given approval to the final version of the manuscript.

### Notes

The authors declare no competing financial interest.

## ■ ACKNOWLEDGMENTS

The authors are grateful for support from the NSF Award (DMR-2103722). N.B.S. acknowledges support from the Camille Dreyfus Teaching-Scholar Award supported by the Camille and Henry Dreyfus Foundation, and the Hans-Fischer Fellowship. N.B.S. is also grateful for support from the Friedrich Wilhelm Bessel Research Award and the Alexander von Humboldt Foundation. G.C.T. is supported by the National Science Foundation's Graduate Research Fellowship under Grant No. DGE-2034711.

## ■ ABBREVIATIONS

MOF, metal−organic framework; CSO, 1,3,3-trimethylspiro-[indoline-2,3′-naphtho[2,1-*b*][1,4]oxazine]-5-carboxylic acid; NMR, nuclear magnetic resonance; CSP, 1′,3′,3′-trimethyl-6-nitrospiro[chromene-2,2′-indoline]-5′-carboxylic acid; UiO-66, $Zr_6O_4(OH)_4(TA)_6$; TA, terephthalic acid; UiO-67, $Zr_6O_4(OH)_4(BPDC)_6$; $H_2BPDC$, 1,4-biphenyldicarboxylic acid; UiO-68, $Zr_6O_4(OH)_4(NBB)_6$; $H_2NBB$, 4,4′-(naphthalene-1,4-diyl)dibenzoic acid; NU-1000, $Zr_6O_4(OH)_8(TBAPy)_2$; $H_4TBAPy$, 1,3,6,8-tetrakis(*p*-benzoic acid)pyrene; PXRD, powder X-ray diffraction; TGA, thermogravimetric analysis; DMF, *N*,*N*-dimethylformamide; THF, tetrahydrofuran; DEF, *N*,*N*-diethylformamide; BuOH, butanol; EA, ethyl acetate; COF, covalent-organic framework

## ■ REFERENCES

(1) Li, W.-X.; Yin, Y.-F.; Duan, H.-Y.; Liu, L.-J.; Kong, L.-C.; Zhan, T.-G.; Zhang, K.-D. An Orthogonal Photoresponsive Tristable [3]Rotaxane with Non-Destructive Readout. *Org. Chem. Front.* **2021**, *8*, 1482−1489.
(2) Meng, F.; Hervault, Y.-M.; Shao, Q.; Hu, B.; Norel, L.; Rigaut, S.; Chen, X. Orthogonally Modulated Molecular Transport Junctions for Resettable Electronic Logic Gates. *Nat. Commun.* **2014**, *5*, No. 3023.
(3) Aprahamian, I. The Future of Molecular Machines. *ACS Cent. Sci.* **2020**, *6*, 347−358.
(4) Iagatti, A.; Shao, B.; Credi, A.; Ventura, B.; Aprahamian, I.; Donato, M. D. Ultrafast Processes Triggered by One- and Two-Photon Excitation of a Photochromic and Luminescent Hydrazone. *Beilstein J. Org. Chem.* **2019**, *15*, 2438−2446.
(5) Moody, G.; Islam, M. S. Materials for Ultra-Efficient, High-Speed Optoelectronics. *MRS Bull.* **2022**, *47*, 475−484.
(6) Rad, J. K.; Balzade, Z.; Mahdavian, A. R. Spiropyran-Based Advanced Photoswitchable Materials: A Fascinating Pathway to the Future Stimuli-Responsive Devices. *J. Photochem. Photobiol., C* **2022**, *51*, No. 100487.
(7) Garai, B.; Mallick, A.; Banerjee, R. Photochromic Metal−Organic Frameworks for Inkless and Erasable Printing. *Chem. Sci.* **2016**, *7*, 2195−2200.
(8) Thaggard, G. C.; Kankanamalage, B. K. P. M.; Park, K. C.; Haimerl, J.; Fischer, R. A.; Shustova, N. B. Switching in Harmony: Tailoring the Properties of Functional Materials with Orthogonal Stimuli. *Chem. Phys. Rev.* **2024**, *5*, No. 011305.
(9) Green, K. A.; Cifuentes, M. P.; Corkery, T. C.; Samoc, M.; Humphrey, M. G. Switching the Cubic Nonlinear Optical Properties of an Electro-, Halo-, and Photochromic Ruthenium Alkynyl Complex Across Six States. *Angew. Chem., Int. Ed.* **2009**, *48*, 7867−7870.
(10) Karmakar, M.; Bag, S. K.; Mondal, B.; Thakur, A. A Conjugated Photoresponsive Dithienylethene−Ferrocene System: Applications in Secret Writing and Decoding Information. *J. Mater. Chem. C* **2022**, *10*, 8860−8873.
(11) Li, Z.; Wang, G.; Ye, Y.; Li, B.; Li, H.; Chen, B. Loading Photochromic Molecules into a Luminescent Metal−Organic Framework for Information Anticounterfeiting. *Angew. Chem., Int. Ed.* **2019**, *58*, 18025−18031.
(12) Zhang, D.; Zhang, Y.; Gong, W.; Li, J.; Liu, S.; Ma, Y.; Zhao, Q. Manipulating Photoisomerization Rate of Triphenylethylene Derivative through Metal Coordination for Irradiation Time-Dependent Information Encryption. *Adv. Opt. Mater.* **2023**, *11*, No. 2300386.
(13) Su, J.; Yuan, S.; Li, J.; Wang, H.-Y.; Ge, J.-Y.; Drake, H. F.; Leong, C. F.; Yu, F.; D'Alessandro, D. M.; Kurmoo, M.; Zuo, J.-L.; Zhou, H.-C. Rare-Earth Metal Tetrathiafulvalene Carboxylate Frameworks as Redox-Switchable Single-Molecule Magnets. *Chem. - Eur. J.* **2021**, *27*, 622−627.
(14) Le, M.; Han, G. G. D. Stimuli-Responsive Organic Phase Change Materials: Molecular Designs and Applications in Energy Storage. *Acc. Mater. Res.* **2022**, *3*, 634−643.
(15) Zhang, B.; Feng, Y.; Feng, W. Azobenzene-Based Solar Thermal Fuels: A Review. *Nano-Micro Lett.* **2022**, *14*, No. 138.
(16) Wu, S.; Li, T.; Zhang, Z.-Y.; Li, T.; Wang, R. Photoswitchable Phase Change Materials for Unconventional Thermal Energy Storage and Upgrade. *Matter* **2021**, *4*, 3385−3399.
(17) Williams, D. E.; Rietman, J. A.; Maier, J. M.; Tan, R.; Greytak, A. B.; Smith, M. D.; Krause, J. A.; Shustova, N. B. Energy Transfer on Demand: Photoswitch-Directed Behavior of Metal−Porphyrin Frameworks. *J. Am. Chem. Soc.* **2014**, *136*, 11886−11889.
(18) Qiu, Q.; Sun, Z.; Joubran, D.; Li, X.; Wan, J.; Schmidt-Rohr, K.; Han, G. G. D. Optically Controlled Recovery and Recycling of Homogeneous Organocatalysts Enabled by Photoswitches. *Angew. Chem., Int. Ed.* **2023**, *62*, No. e202300723.
(19) DiNardi, R. G.; Rasheed, S.; Capomolla, S. S.; Chak, M. H.; Middleton, I. A.; Macreadie, L. K.; Violi, J. P.; Donald, W. A.; Lusby, P. J.; Beves, J. E. Photoswitchable Catalysis by a Self-Assembled Molecular Cage. *J. Am. Chem. Soc.* **2024**, *146*, 21196−21202.
(20) Shin, J.; Sung, J.; Kang, M.; Xie, X.; Lee, B.; Lee, K. M.; White, T. J.; Leal, C.; Sottos, N. R.; Braun, P. V.; Cahill, D. G. Light-Triggered Thermal Conductivity Switching in Azobenzene Polymers. *Proc. Natl. Acad. Sci. U.S.A.* **2019**, *116*, 5973−5978.
(21) Müller, K.; Helfferich, J.; Zhao, F.; Verma, R.; Kanj, A. B.; Meded, V.; Bléger, D.; Wenzel, W.; Heinke, L. Switching the Proton Conduction in Nanoporous, Crystalline Materials by Light. *Adv. Mater.* **2018**, *30*, No. 1706551.
(22) Dolgopolova, E. A.; Galitskiy, V. A.; Martin, C. R.; Gregory, H. N.; Yarbrough, B. J.; Rice, A. M.; Berseneva, A. A.; Ejegbavwo, O. A.; Stephenson, K. S.; Kittikhunnatham, P.; Karakalos, S. G.; Smith, M. D.; Greytak, A. B.; Garashchuk, S.; Shustova, N. B. Connecting Wires: Photoinduced Electronic Structure Modulation in Metal−Organic Frameworks. *J. Am. Chem. Soc.* **2019**, *141*, 5350−5358.
(23) Martin, C. R.; Park, K. C.; Leith, G. A.; Yu, J.; Mathur, A.; Wilson, G. R.; Gange, G. B.; Barth, E. L.; Ly, R. T.; Manley, O. M.; Forrester, K. L.; Karakalos, S. G.; Smith, M. D.; Makris, T. M.; Vannucci, A. K.; Peryshkov, D. V.; Shustova, N. B. Stimuli-Modulated Metal Oxidation States in Photochromic MOFs. *J. Am. Chem. Soc.* **2022**, *144*, 4457−4468.
(24) Dolgopolova, E. A.; Berseneva, A. A.; Faillace, M. S.; Ejegbavwo, O. A.; Leith, G. A.; Choi, S. W.; Gregory, H. N.; Rice, A. M.; Smith, M. D.; Chruszcz, M.; Garashchuk, S.; Mythreye, K.; Shustova, N. B. Confinement-Driven Photophysics in Cages, Covalent−Organic Frameworks, Metal−Organic Frameworks, and DNA. *J. Am. Chem. Soc.* **2020**, *142*, 4769−4783.
(25) Shao, B.; Baroncini, M.; Qian, H.; Bussotti, L.; Di Donato, M.; Credi, A.; Aprahamian, I. Solution and Solid-State Emission Toggling

of a Photochromic Hydrazone. *J. Am. Chem. Soc.* **2018**, *140*, 12323−12327.
(26) Gonzalez, A.; Kengmana, E. S.; Fonseca, M. V.; Han, G. G. D. Solid-State Photoswitching Molecules: Structural Design for Isomerization in Condensed Phase. *Mater. Today Adv.* **2020**, *6*, No. 100058.
(27) Klajn, R. Spiropyran-Based Dynamic Materials. *Chem. Soc. Rev.* **2014**, *43*, 148−184.
(28) Shao, B.; Aprahamian, I. Hydrazones as New Molecular Tools. *Chem* **2020**, *6*, 2162−2173.
(29) Yaghi, O. M. Reticular Chemistry in All Dimensions. *ACS Cent. Sci.* **2019**, *5*, 1295−1300.
(30) Ji, Z.; Wang, H.; Canossa, S.; Wuttke, S.; Yaghi, O. M. Pore Chemistry of Metal−Organic Frameworks. *Adv. Funct. Mater.* **2020**, *30*, No. 2000238.
(31) Wang, W.; Chen, Y.; Feng, P.; Bu, X. Tailorable Multi-Modular Pore-Space-Partitioned Vanadium Metal-Organic Frameworks for Gas Separation. *Adv. Mater.* **2024**, *36*, No. 2403834.
(32) Son, F. A.; Bailey, O. J.; Islamoglu, T.; Farha, O. K. Decorating the Node of a Zirconium-Based Metal−Organic Framework to Tune Adsorption Behavior and Surface Permeation. *ACS Appl. Mater. Interfaces* **2024**, *16*, 31798−31806.
(33) Yaghi, O. M.; Kalmutzki, M. J.; Diercks, C. S. Building Units of MOFs. In *Introduction to Reticular Chemistry*; John Wiley & Sons, Ltd, 2019; pp 57−81.
(34) Fiankor, C.; Nyakuchena, J.; Khoo, R. S. H.; Zhang, X.; Hu, Y.; Yang, S.; Huang, J.; Zhang, J. Symmetry-Guided Synthesis of *N,N′*-Bicarbazole and Porphyrin-Based Mixed-Ligand Metal−Organic Frameworks: Light Harvesting and Energy Transfer. *J. Am. Chem. Soc.* **2021**, *143*, 20411−20418.
(35) Liu, Y.; Howarth, A. J.; Hupp, J. T.; Farha, O. K. Selective Photooxidation of a Mustard-Gas Simulant Catalyzed by a Porphyrinic Metal−Organic Framework. *Angew. Chem., Int. Ed.* **2015**, *54*, 9001−9005.
(36) Kim, T. K.; Lee, K. J.; Cheon, J. Y.; Lee, J. H.; Joo, S. H.; Moon, H. R. Nanoporous Metal Oxides with Tunable and Nanocrystalline Frameworks via Conversion of Metal−Organic Frameworks. *J. Am. Chem. Soc.* **2013**, *135*, 8940−8946.
(37) Nam, K. W.; Park, S. S.; dos Reis, R.; Dravid, V. P.; Kim, H.; Mirkin, C. A.; Stoddart, J. F. Conductive 2D Metal-Organic Framework for High-Performance Cathodes in Aqueous Rechargeable Zinc Batteries. *Nat. Commun.* **2019**, *10*, No. 4948.
(38) Ehrling, S.; Reynolds, E. M.; Bon, V.; Senkovska, I.; Gorelik, T. E.; Evans, J. D.; Rauche, M.; Mendt, M.; Weiss, M. S.; Pöppl, A.; Brunner, E.; Kaiser, U.; Goodwin, A. L.; Kaskel, S. Adaptive Response of a Metal−Organic Framework through Reversible Disorder−Disorder Transitions. *Nat. Chem.* **2021**, *13*, 568−574.
(39) Bicalho, H. A.; Saraci, F.; de J Velazquez-Garcia, J.; Titi, H. M.; Howarth, A. J. Unravelling the Synthesis of a Rare-Earth Cluster-Based Metal−Organic Framework with Spn Topology. *Chem. Commun.* **2022**, *58*, 10925−10928.
(40) Howarth, A. J.; Liu, Y.; Li, P.; Li, Z.; Wang, T. C.; Hupp, J. T.; Farha, O. K. Chemical, Thermal and Mechanical Stabilities of Metal−Organic Frameworks. *Nat. Rev. Mater.* **2016**, *1*, No. 15018.
(41) Zheng, T.; Yang, Z.; Gui, D.; Liu, Z.; Wang, X.; Dai, X.; Liu, S.; Zhang, L.; Gao, Y.; Chen, L.; Sheng, D.; Wang, Y.; Diwu, J.; Wang, J.; Zhou, R.; Chai, Z.; Albrecht-Schmitt, T. E.; Wang, S. Overcoming the Crystallization and Designability Issues in the Ultrastable Zirconium Phosphonate Framework System. *Nat. Commun.* **2017**, *8*, No. 15369.
(42) Dou, J.-H.; Arguilla, M. Q.; Luo, Y.; Li, J.; Zhang, W.; Sun, L.; Mancuso, J. L.; Yang, L.; Chen, T.; Parent, L. R.; Skorupskii, G.; Libretto, N. J.; Sun, C.; Yang, M. C.; Dip, P. V.; Brignole, E. J.; Miller, J. T.; Kong, J.; Hendon, C. H.; Sun, J.; Dincă, M. Atomically Precise Single-Crystal Structures of Electrically Conducting 2D Metal−Organic Frameworks. *Nat. Mater.* **2021**, *20*, 222−228.
(43) Zhai, Q.-G.; Bu, X.; Mao, C.; Zhao, X.; Daemen, L.; Cheng, Y.; Ramirez-Cuesta, A. J.; Feng, P. An Ultra-Tunable Platform for Molecular Engineering of High-Performance Crystalline Porous Materials. *Nat. Commun.* **2016**, *7*, No. 13645.
(44) Li, L.; Guo, L.; Olson, D. H.; Xian, S.; Zhang, Z.; Yang, Q.; Wu, K.; Yang, Y.; Bao, Z.; Ren, Q.; Li, J. Discrimination of Xylene Isomers in a Stacked Coordination Polymer. *Science* **2022**, *377*, 335−339.
(45) Lu, Z.; Duan, J.; Tan, H.; Du, L.; Zhao, X.; Wang, R.; Kato, S.; Yang, S.; Hupp, J. T. Isomer of NU-1000 with a Blocking c-pore Exhibits High Water−Vapor Uptake Capacity and Greatly Enhanced Cycle Stability. *J. Am. Chem. Soc.* **2023**, *145*, 4150−4157.
(46) Nyakuchena, J.; Ostresh, S.; Streater, D.; Pattengale, B.; Neu, J.; Fiankor, C.; Hu, W.; Kinigstein, E. D.; Zhang, J.; Zhang, X.; Schmuttenmaer, C. A.; Huang, J. Direct Evidence of Photoinduced Charge Transport Mechanism in 2D Conductive Metal Organic Frameworks. *J. Am. Chem. Soc.* **2020**, *142*, 21050−21058.
(47) Pham, H. T. B.; Choi, J. Y.; Huang, S.; Wang, X.; Claman, A.; Stodolka, M.; Yazdi, S.; Sharma, S.; Zhang, W.; Park, J. Imparting Functionality and Enhanced Surface Area to a 2D Electrically Conductive MOF via Macrocyclic Linker. *J. Am. Chem. Soc.* **2022**, *144*, 10615−10621.
(48) Chen, Z.; Li, P.; Anderson, R.; Wang, X.; Zhang, X.; Robison, L.; Redfern, L. R.; Moribe, S.; Islamoglu, T.; Gómez-Gualdrón, D. A.; Yildirim, T.; Stoddart, J. F.; Farha, O. K. Balancing Volumetric and Gravimetric Uptake in Highly Porous Materials for Clean Energy. *Science* **2020**, *368*, 297−303.
(49) Choe, M.; Koo, J. Y.; Park, I.; Ohtsu, H.; Shim, J. H.; Choi, H. C.; Park, S. S. Chemical Vapor Deposition of Edge-on Oriented 2D Conductive Metal−Organic Framework Thin Films. *J. Am. Chem. Soc.* **2022**, *144*, 16726−16731.
(50) Hanikel, N.; Pei, X.; Chheda, S.; Lyu, H.; Jeong, W.; Sauer, J.; Gagliardi, L.; Yaghi, O. M. Evolution of Water Structures in Metal-Organic Frameworks for Improved Atmospheric Water Harvesting. *Science* **2021**, *374*, 454−459.
(51) Abylgazina, L.; Senkovska, I.; Kaskel, S. Logic and Symbolism of Switchable Porous Framework Materials. *Commun. Mater.* **2024**, *5*, No. 132.
(52) Cerasale, D. J.; Ward, D. C.; Easun, T. L. MOFs in the Time Domain. *Nat. Rev. Chem.* **2022**, *6*, 9−30.
(53) Asghar, A.; Iqbal, N.; Noor, T.; Kariuki, B. M.; Kidwell, L.; Easun, T. L. Efficient Electrochemical Synthesis of a Manganese-Based Metal−Organic Framework for $H_2$ and $CO_2$ Uptake. *Green Chem.* **2021**, *23*, 1220−1227.
(54) Chen, W.; Cai, P.; Elumalai, P.; Zhang, P.; Feng, L.; Al-Rawashdeh, M.; Madrahimov, S. T.; Zhou, H.-C. Site-Isolated Azobenzene-Containing Metal−Organic Framework for Cyclopalladated Catalyzed Suzuki-Miyuara Coupling in Flow. *ACS Appl. Mater. Interfaces* **2021**, *13*, 51849−51854.
(55) Drake, H. F.; Day, G. S.; Xiao, Z.; Zhou, H.-C.; Ryder, M. R. Light-Induced Switchable Adsorption in Azobenzene- and Stilbene-Based Porous Materials. *Trends Chem.* **2022**, *4*, 32−47.
(56) Brown, J. W.; Henderson, B. L.; Kiesz, M. D.; Whalley, A. C.; Morris, W.; Grunder, S.; Deng, H.; Furukawa, H.; Zink, J. I.; Stoddart, J. F.; Yaghi, O. M. Photophysical Pore Control in an Azobenzene-Containing Metal−Organic Framework. *Chem. Sci.* **2013**, *4*, 2858−2864.
(57) Thaggard, G. C.; Leith, G. A.; Sosnin, D.; Martin, C. R.; Park, K. C.; McBride, M. K.; Lim, J.; Yarbrough, B. J.; Kankanamalage, B. K. P. M.; Wilson, G. R.; Hill, A. R.; Smith, M. D.; Garashchuk, S.; Greytak, A. B.; Aprahamian, I.; Shustova, N. B. Confinement-Driven Photophysics in Hydrazone-Based Hierarchical Materials. *Angew. Chem., Int. Ed.* **2023**, *62*, No. e202211776.
(58) Williams, D. E.; Martin, C. R.; Dolgopolova, E. A.; Swifton, A.; Godfrey, D. C.; Ejegbavwo, O. A.; Pellechia, P. J.; Smith, M. D.; Shustova, N. B. Flipping the Switch: Fast Photoisomerization in a Confined Environment. *J. Am. Chem. Soc.* **2018**, *140*, 7611−7622.
(59) Thaggard, G. C.; Haimerl, J.; Park, K. C.; Lim, J.; Fischer, R. A.; Kankanamalage, B. K. P. M.; Yarbrough, B. J.; Wilson, G. R.; Shustova, N. B. Metal−Photoswitch Friendship: From Photochromic Complexes to Functional Materials. *J. Am. Chem. Soc.* **2022**, *144*, 23249−23263.
(60) Grommet, A. B.; Lee, L. M.; Klajn, R. Molecular Photoswitching in Confined Spaces. *Acc. Chem. Res.* **2020**, *53*, 2600−2610.

(61) Thaggard, G. C.; Park, K. C.; Lim, J.; Kankanamalage, B. K. P. M.; Haimerl, J.; Wilson, G. R.; McBride, M. K.; Forrester, K. L.; Adelson, E. R.; Arnold, V. S.; Wetthasinghe, S. T.; Rassolov, V. A.; Smith, M. D.; Sosnin, D.; Aprahamian, I.; Karmakar, M.; Bag, S. K.; Thakur, A.; Zhang, M.; Tang, B. Z.; Castaño, J. A.; Chaur, M. N.; Lerch, M. M.; Fischer, R. A.; Aizenberg, J.; Herges, R.; Lehn, J.-M.; Shustova, N. B. Breaking the Photoswitch Speed Limit. *Nat. Commun.* **2023**, *14*, No. 7556.
(62) Isokuortti, J.; Kuntze, K.; Virkki, M.; Ahmed, Z.; Vuorimaa-Laukkanen, E.; Filatov, M. A.; Turshatov, A.; Laaksonen, T.; Priimagi, A.; Durandin, N. A. Expanding Excitation Wavelengths for Azobenzene Photoswitching into the Near-Infrared Range via Endothermic Triplet Energy Transfer. *Chem. Sci.* **2021**, *12*, 7504−7509.
(63) Zhu, Q.; Wang, S.; Chen, P. Diazocine Derivatives: A Family of Azobenzenes for Photochromism with Highly Enhanced Turn-On Fluorescence. *Org. Lett.* **2019**, *21*, 4025−4029.
(64) Orvoš, J.; Fischer, R.; Brachňaková, B.; Pavlik, J.; Moncoľ, J.; Šagátová, A.; Fronc, M.; Kožíšek, J.; Routaboul, L.; Bousseksou, A.; Šalitroš, I. Pyridyl-Benzimidazole Derivatives Decorated with Phenylazo Substituents and Their Low-Spin Iron(ii) Complexes: A Study of the Synthesis, Structure and Photoisomerization. *New J. Chem.* **2023**, *47*, 1488−1497.
(65) Saha, M.; Ghosh, S.; Bandyopadhyay, S. Strain, Switching and Fluorescence Behavior of a Nine-Membered Cyclic Azobenzene. *New J. Chem.* **2018**, *42*, 10784−10790.
(66) Pirone, D.; Bandeira, N. A. G.; Tylkowski, B.; Boswell, E.; Labeque, R.; Valls, R. G.; Giamberini, M. Contrasting Photo-Switching Rates in Azobenzene Derivatives: How the Nature of the Substituent Plays a Role. *Polymers* **2020**, *12*, No. 1019.
(67) Chaur, M. N.; Collado, D.; Lehn, J.-M. Configurational and Constitutional Information Storage: Multiple Dynamics in Systems Based on Pyridyl and Acyl Hydrazones. *Chem. - Eur. J.* **2011**, *17*, 248−258.
(68) Zhang, M.; Zhang, J.; Alam, P.; Li, W.; Lam, J. W. Y.; Jia, G.; Tang, B. Z. Hydrazone-Based AIEgens with Photofluorochromic Ability for Rewritable, Intensity-Variable, and High-Resolution Photopattern. *Adv. Funct. Mater.* **2023**, *33*, No. 2213927.
(69) Larsson, W.; Morimoto, M.; Irie, M.; Andréasson, J.; Albinsson, B. Diarylethene Isomerization by Using Triplet−Triplet Annihilation Photon Upconversion. *Chem. - Eur. J.* **2023**, *29*, No. e202203651.
(70) Sanjabi, S.; Alinejad, Z.; Mouraki, A.; Mahdavian, A. R. Controlled Photoisomerization in Acrylic Copolymer Nanoparticles Based on Spironaphthoxazine for Reduced Thermal Reversion. *Eur. Polym. J.* **2019**, *119*, 487−498.
(71) Zhang, P.; Meng, J.; Li, X.; Wang, Y.; Matsuura, T. Synthesis and Photochromism of Photochromic Spiro Compounds Having a Reactive Pendant Group. *J. Heterocycl. Chem.* **2002**, *39*, 179−184.
(72) Schwartz, H. A.; Werker, M.; Tobeck, C.; Christoffels, R.; Schaniel, D.; Olthof, S.; Meerholz, K.; Kopacka, H.; Huppertz, H.; Ruschewitz, U. Novel Photoactive Spirooxazine Based Switch@MOF Composite Materials. *ChemPhotoChem* **2020**, *4*, 195−206.
(73) Gao, H.; Yuan, L.; Liu, G.; Gao, J. An Ultraviolet Light-Responsive Polyacrylate Film with High Fatigue Resistance. *J. Polym. Res.* **2022**, *29*, No. 46.
(74) Das, G.; Prakasam, T.; Alkhatib, N.; AbdulHalim, R. G.; Chandra, F.; Sharma, S. K.; Garai, B.; Varghese, S.; Addicoat, M. A.; Ravaux, F.; Pasricha, R.; Jagannathan, R.; Saleh, N.; Kirmizialtin, S.; Olson, M. A.; Trabolsi, A. Light-Driven Self-Assembly of Spiropyran-Functionalized Covalent Organic Framework. *Nat. Commun.* **2023**, *14*, No. 3765.
(75) Zheng, H.-Q.; Yang, Y.; Wang, Z.; Yang, D.; Qian, G.; Cui, Y. Photo-Stimuli-Responsive Dual-Emitting Luminescence of a Spiropyran-Encapsulating Metal−Organic Framework for Dynamic Information Encryption. *Adv. Mater.* **2023**, *35*, No. 2300177.
(76) Xia, H.; Xie, K.; Zou, G. Advances in Spiropyrans/Spirooxazines and Applications Based on Fluorescence Resonance Energy Transfer (FRET) with Fluorescent Materials. *Molecules* **2017**, *22*, No. 2236.
(77) Berkovic, G.; Krongauz, V.; Weiss, V. Spiropyrans and Spirooxazines for Memories and Switches. *Chem. Rev.* **2000**, *100*, 1741−1754.
(78) Kortekaas, L.; Browne, W. S. The Evolution of Spiropyran: Fundamentals and Progress of an Extraordinarily Versatile Photochrome. *Chem. Soc. Rev.* **2019**, *48*, 3406−3424.
(79) Marevtsev, V. S.; Zaichenko, N. L. Peculiarities of Photochromic Behaviour of Spiropyrans and Spirooxazines. *J. Photochem. Photobiol. A Chem.* **1997**, *104*, 197−202.
(80) Fan, C. B.; Liu, Z. Q.; Gong, L. L.; Zheng, A. M.; Zhang, L.; Yan, C. S.; Wu, H. Q.; Feng, X. F.; Luo, F. Photoswitching Adsorption Selectivity in a Diarylethene−Azobenzene MOF. *Chem. Commun.* **2017**, *53*, 763−766.
(81) Hoang, L. T. M.; Ngo, L. H.; Nguyen, H. L.; Nguyen, H. T. H.; Nguyen, C. K.; Nguyen, B. T.; Ton, Q. T.; Nguyen, H. K. D.; Cordova, K. E.; Truong, T. An Azobenzene-Containing Metal−Organic Framework as an Efficient Heterogeneous Catalyst for Direct Amidation of Benzoic Acids: Synthesis of Bioactive Compounds. *Chem. Commun.* **2015**, *51*, 17132−17135.
(82) Wang, Z.; Müller, K.; Valášek, M.; Grosjean, S.; Bräse, S.; Wöll, C.; Mayor, M.; Heinke, L. Series of Photoswitchable Azobenzene-Containing Metal−Organic Frameworks with Variable Adsorption Switching Effect. *J. Phys. Chem. C* **2018**, *122*, 19044−19050.
(83) Sasai, R.; Shinomura, H. Preparation and Optical Characteristics of Layered Perovskite-Type Lead-Bromide-Incorporated Azobenzene Chromophores. *J. Solid State Chem.* **2013**, *198*, 452−458.
(84) Zampini, G.; Ortica, F.; Cannavale, A.; Latterini, L. Spirooxazine Loading Effects on the Photochromism of Polymer Films. *Dyes Pigm.* **2023**, *210*, No. 111018.
(85) Zhang, T.; Lou, X.-Y.; Li, X.; Tu, X.; Han, J.; Zhao, B.; Yang, Y.-W. Tunable Photochromism of Spirooxazine in the Solid State: A New Design Strategy Based on the Hypochromic Effect. *Adv. Mater.* **2023**, *35*, No. 2210551.
(86) Morsümbül, S.; Kumbasar, E. P. A.; Kıyak, S. A.; Alemdar, I. G. A New Approach to Photochromic Nanofiber-Based Ultraviolet Sensors with Grayscale Adaptation. *Polym. Eng. Sci.* **2024**, *64*, 4246−4257.
(87) Kim, S.-H.; Choi, S.-W.; Suh, H.-J.; Jin, S.-H.; Gal, Y.-S.; Koh, K. Surface Plasmon Resonance Spectroscopy on the Interaction of a Self-Assembled Monolayer with Linear Hydrocarbon Such as Pentane, Hexane, Heptane and Octane. *Dyes Pigm.* **2002**, *55*, 17−25.
(88) Kim, S.-H.; Ock, K.-S.; Kim, J.-H.; Koh, K.-N.; Kang, S.-W. Optical Properties and Molecular Orientation of Self-Assembled Monolayer Using Surface Plasmon Resonance Spectroscopy. *Dyes Pigm.* **2001**, *48*, 1−6.
(89) Wu, Z.; Pan, K.; Mo, S.; Wang, B.; Zhao, X.; Yin, M. Tetraphenylethene-Induced Free Volumes for the Isomerization of Spiropyran toward Multifunctional Materials in the Solid State. *ACS Appl. Mater. Interfaces* **2018**, *10*, 30879−30886.
(90) Park, K. C.; Martin, C. R.; Leith, G. A.; Thaggard, G. C.; Wilson, G. R.; Yarbrough, B. J.; Kankanamalage, B. K. P. M.; Kittikhunnatham, P.; Mathur, A.; Jatoi, I.; Manzi, M. A.; Lim, J.; Lehman-Andino, I.; Hernandez-Jimenez, A.; Amoroso, J. W.; DiPrete, D. P.; Liu, Y.; Schaeperkoetter, J.; Misture, S. T.; Phillpot, S. R.; Hu, S.; Li, Y.; Leydier, A.; Proust, V.; Grandjean, A.; Smith, M. D.; Shustova, N. B. Capture Instead of Release: Defect-Modulated Radionuclide Leaching Kinetics in Metal−Organic Frameworks. *J. Am. Chem. Soc.* **2022**, *144*, 16139−16149.
(91) Larkowska, M.; Wuebbenhorst, M.; Kucharski, S. Spirooxazine Photoisomerization and Relaxation in Polymer Matrices. *Int. J. Polym. Sci.* **2011**, *2011*, No. 627195.
(92) Whelan, J.; Abdallah, D.; Piskorz, K.; Wojtyk, J. T. C.; Dust, J. M.; Nunzi, J.-M.; Hoz, S.; Buncel, E. Photochemical and Thermal Spiropyran (SP)-Merocyanine (MC) Interconversion: A Dichotomy in Dependence on Viscosity. *Phys. Chem. Chem. Phys.* **2012**, *14*, 13684−13691.
(93) Shiraishi, Y.; Inoue, T.; Sumiya, S.; Hirai, T. Entropy-Driven Thermal Isomerization of Spiropyran in Viscous Media. *J. Phys. Chem. A* **2011**, *115*, 9083−9090.


https://doi.org/10.1021/jacs.4c10636
J. Am. Chem. Soc. 2024, 146, 31746−31756

(94) Savchenko, V.; Lomadze, N.; Santer, S.; Guskova, O. Spiropyran/Merocyanine Amphiphile in Various Solvents: A Joint Experimental−Theoretical Approach to Photophysical Properties and Self-Assembly. *Int. J. Mol. Sci.* **2022**, *23*, No. 11535.
(95) Frassi, D.; Padula, G.; Granucci, G. Photoisomerization of Spiropyran in Solution: A Surface Hopping Investigation. *J. Phys. Chem. B* **2024**, *128*, 5246−5253.
(96) Wang, J.; Avram, L.; Diskin-Posner, Y.; Białek, M. J.; Stawski, W.; Feller, M.; Klajn, R. Altering the Properties of Spiropyran Switches Using Coordination Cages with Different Symmetries. *J. Am. Chem. Soc.* **2022**, *144*, 21244−21254.
(97) Dünnebacke, T.; Kartha, K. K.; Wahl, J. M.; Albuquerque, R. Q.; Fernández, G. Solvent-Controlled *E*/*Z* Isomerization vs. [2 + 2] Photocycloaddition Mediated by Supramolecular Polymerization. *Chem. Sci.* **2020**, *11*, 10405−10413.
(98) Mamun, M. S. A.; Sainoo, Y.; Takaoka, T.; Waizumi, H.; Wang, Z.; Alam, M. I.; Ando, A.; Arafune, R.; Komeda, T. Chemistry of the Photoisomerization and Thermal Reset of Nitro-Spiropyran and Merocyanine Molecules on the Channel of the $MoS_2$ Field Effect Transistor. *Phys. Chem. Chem. Phys.* **2021**, *23*, 27273−27281.
(99) Gaeva, E. B.; Pimienta, V.; Metelitsa, A. V.; Voloshin, N. A.; Minkin, V. I.; Micheau, J. C. Solvation Effects on Spirooxazine to Merocyanine Thermal Reversion Kinetics in Acetonitrile−Water Binary Mixtures. *J. Phys. Org. Chem.* **2005**, *18*, 315−320.
(100) Khairutdinov, R. F.; Giertz, K.; Hurst, J. K.; Voloshina, E. N.; Voloshin, N. A.; Minkin, V. I. Photochromism of Spirooxazines in Homogeneous Solution and Phospholipid Liposomes. *J. Am. Chem. Soc.* **1998**, *120*, 12707−12713.
(101) Wang, K.-Y.; Yang, Z.; Zhang, J.; Banerjee, S.; Joseph, E. A.; Hsu, Y.-C.; Yuan, S.; Feng, L.; Zhou, H.-C. Creating Hierarchical Pores in Metal−Organic Frameworks via Postsynthetic Reactions. *Nat. Protoc.* **2023**, *18*, 604−625.
(102) Katz, M. J.; Brown, Z. J.; Colón, Y. J.; Siu, P. W.; Scheidt, K. A.; Snurr, R. Q.; Hupp, J. T.; Farha, O. K. A Facile Synthesis of UiO-66, UiO-67 and Their Derivatives. *Chem. Commun.* **2013**, *49*, 9449−9451.
(103) Gosselin, A. J.; Decker, G. E.; McNichols, B. W.; Baumann, J. E.; Yap, G. P. A.; Sellinger, A.; Bloch, E. D. Ligand-Based Phase Control in Porous Zirconium Coordination Cages. *Chem. Mater.* **2020**, *32*, 5872−5878.
(104) Wang, T. C.; Vermeulen, N. A.; Kim, I. S.; Martinson, A. B. F.; Stoddart, J. F.; Hupp, J. T.; Farha, O. K. Scalable Synthesis and Post-Modification of a Mesoporous Metal-Organic Framework Called NU-1000. *Nat. Protoc.* **2016**, *11*, 149−162.
(105) Valenzano, L.; Civalleri, B.; Chavan, S.; Bordiga, S.; Nilsen, M. H.; Jakobsen, S.; Lillerud, K. P.; Lamberti, C. Disclosing the Complex Structure of UiO-66 Metal Organic Framework: A Synergic Combination of Experiment and Theory. *Chem. Mater.* **2011**, *23*, 1700−1718.
(106) Osella, S.; Granucci, G.; Persico, M.; Knippenberg, S. Dual Photoisomerization Mechanism of Azobenzene Embedded in a Lipid Membrane. *J. Mater. Chem. B* **2023**, *11*, 2518−2529.
(107) Samanta, D.; Galaktionova, D.; Gemen, J.; Shimon, L. J. W.; Diskin-Posner, Y.; Avram, L.; Král, P.; Klajn, R. Reversible Chromism of Spiropyran in the Cavity of a Flexible Coordination Cage. *Nat. Commun.* **2018**, *9*, No. 641.
(108) Sun, F.; Xiong, X.; Gao, A.; Duan, Y.; Mao, L.; Gu, L.; Wang, Z.; He, C.; Deng, X.; Zheng, Y.; Wang, D. Fast Photochromism in Solid: Microenvironment in Metal-Organic Frameworks Promotes the Isomerization of Donor-Acceptor Stenhouse Adducts. *Chem. Eng. J.* **2022**, *427*, No. 132037.
(109) Mollick, S.; Zhang, Y.; Kamal, W.; Tricarico, M.; Möslein, A. F.; Kachwal, V.; Amin, N.; Castrejón-Pita, A. A.; Morris, S. M.; Tan, J.-C. Resilient Photoswitchable Metal−Organic Frameworks for Sunlight-Induced on-Demand Photochromism in the Solid State. *Chem. Eng. J.* **2023**, *476*, No. 146727.
(110) Stanley, P. M.; Su, A. Y.; Ramm, V.; Fink, P.; Kimna, C.; Lieleg, O.; Elsner, M.; Lercher, J. A.; Rieger, B.; Warnan, J.; Fischer, R. A. Photocatalytic $CO_2$-to-Syngas Evolution with Molecular Catalyst Metal-Organic Framework Nanozymes. *Adv. Mater.* **2023**, *35*, No. 2207380.
(111) Wang, J.; Ji, H.; Guo, Y.; Wang, B.; Han, X.; Li, L.; Wu, F.; Li, J.; Lu, C. Light-Assisted Anti-Wrinkling on Azobenzene-Containing Polyblend Films. *Soft Matter* **2022**, *18*, 4475−4482.
(112) Chibisov, A. K.; Görner, H. Photoprocesses in Spirooxazines and Their Merocyanines. *J. Phys. Chem. A* **1999**, *103*, 5211−5216.
(113) Meeks, A.; Lerch, M. M.; Schroeder, T. B. H.; Shastri, A.; Aizenberg, J. Spiropyran Photoisomerization Dynamics in Multi-responsive Hydrogels. *J. Am. Chem. Soc.* **2022**, *144*, 219−227.
(114) Guo, X.; Shao, B.; Zhou, S.; Aprahamian, I.; Chen, Z. Visualizing Intracellular Particles and Precise Control of Drug Release Using an Emissive Hydrazone Photochrome. *Chem. Sci.* **2020**, *11*, 3016−3021.
(115) Fukaminato, T.; Ishida, S.; Métivier, R. Photochromic Fluorophores at the Molecular and Nanoparticle Levels: Fundamentals and Applications of Diarylethenes. *NPG Asia Mater.* **2018**, *10*, 859−881.
(116) Mandal, M.; Banik, D.; Karak, A.; Manna, S. K.; Mahapatra, A. K. Spiropyran−Merocyanine Based Photochromic Fluorescent Probes: Design, Synthesis, and Applications. *ACS Omega* **2022**, *7*, 36988−37007.


https://doi.org/10.1021/jacs.4c10636
J. Am. Chem. Soc. 2024, 146, 31746−31756